36E.0   IN-SITU CHARACTERIZATION OF MICROSTRUCTURAL EVOLUTION DURING SIMULATED ADDITIVE MANUFACTURING IN MODEL ALLOYS

Brian Rodgers (Mines)
Faculty: Amy Clarke (Mines)
Industrial Mentor: Joe McKeown (LLNL), Edwin Schwalbach (AFRL), Neil Carlson (LANL)

36E.1   Project Overview and Industrial Relevance

Laser Powder Bed Fusion (L-PBF) Additive Manufacturing (AM) is an attractive technology for manufacturing turbine and aerospace components, however, the processing effects of L-PBF on microstructural evolution are not well understood. This project will develop a fundamental understanding of solidification phenomena under AM conditions in model alloys. Emphasis is placed on in-situ experimentation at the Advanced Photon Source (APS) at Argonne National Laboratory (ANL) and Dynamic Transmission Electron Microscopy (DTEM) at Lawrence Livermore National Laboratory (LLNL) with model alloys to understand the role of rapid solidification and processing history on microstructural development. Understanding solidification behavior during L-PBF could allow for enhanced predictive capabilities and microstructural control of components produced by AM.

The model alloy systems chosen are the Al-Ag system and two ternary Ni-base superalloys with different Mo and Al contents, but identical equilibrium γ' volume fractions. The nickel alloys, R2 and R4, are single crystals of known orientation. The Al-Ag system was selected, because it demonstrates strong chemical segregation behavior due to the system's shallow solidus and liquidus slopes. R2 and R4 were chosen for their close resemblance to industrially relevant nickel-based alloys.

36E.2   Previous Work

In-situ experiments at the APS have been performed on alloys in the Al-Ag system and the R2 and R4 alloys. A summary of the alloy compositions and an experimental matrix is provided in tables 36E.1 and 36E.2, respectively. Microstructures of the as-solidified samples were analyzed via scanning electron microscopy (SEM).

Top-down SEM in **Figure 36E.1** of the Al-Ag alloys revealed equiaxed dendrites with six primary arms. There are no planes containing six dendrite growth directions for growth in <100> directions. This phenomenon is explained by <110> growth, which allows for six coplanar primary direction growth directions on {111} planes. Al is an FCC metal, which conventionally means dendritic solidification will proceed along <100> crystallographic directions. The existence of <110> growth direction dendrites implies Dendrite Orientation Transition (DOT) can occur in the Al-Ag system. DOT is a phenomenon where the growth direction of dendrites changes with the addition of solute in certain systems due to changes in the solid-liquid interfacial energy anisotropy [36E.1]. Morphology alone is insufficient to prove growth is proceeding along a given crystallographic direction. Electron diffraction was performed on oriented FIB lit-outs to confirm the growth direction, as shown in **Figure 36E.2**. The analysis confirmed the growth direction as being along <110> in some regions and <100> in others, suggesting DOT exists and is also influenced by local conditions.

Combined SEM and TEM investigation of the Al-Ag samples also revealed some formation mechanisms for γ during solidification and cooling to room temperature. Ag rich regions naturally develop in interdendritic and intercellular regions during cooling, due to partitioning during solidification. As these regions solidify, they will often form γ during solidification, which is expected for this system [36E.2]. Alternatively, γ can be suppressed during solidification, resulting in an α′ region supersaturated in Ag. The region then decomposes into α and γ. Two distinct mechanisms exist by which growth of γ occurs during decomposition, usually simultaneously as shown in **Figure 36E.3**. One method is believed to be via the propagation of ledges, the mechanism for γ growth upon heating a supersaturated solid solution [36E.3]. The method preserves the orientation relationship between the matrix and γ

plates, creating a microstructure with many straight lines. The other method does not maintain the orientation relationship between the α matrix and growing γ, instead developing new branches and curving growth directions.

36E.3 Recent Progress

After discovering DOT in the Al-Ag system, DOT in other systems has become relevant to the scope of this project. DOT in Al-Ge has been reported in the literature [36E.4] and samples in the system have been run in the DTEM. As such, spot melts made with *in-situ* DTEM imaging of Al-Ge have been investigated with TEM, in addition to Al-Ag DTEM samples. Since the DTEM samples are already electron transparent, no preparation is needed before loading a sample into the TEM. Thus, all the DTEM samples analyzed are in the as-solidified state, though there is a layer of nominally amorphous silicon nitride beneath the metal. Additionally, simulations of the thermal history of spot melts in Ni-base superalloys under APS conditions have been performed to determine the thermal gradient for Columnar-to-Equiaxed-Transition (CET) modeling.

36E.3.1 TEM of Al-Ag DTEM

DOT has been confirmed in the APS samples, but the DTEM samples are too thin for convection cells to develop and solidify with a faster interface velocity. There are also no equiaxed dendrites in the Al-Ag DTEM samples. Instead, the bulk of solidification proceeds by the growth of either branchless columnar dendrites or cells. Growth proceeds from the outer edge of the melt pool towards the center for all of the grains; no homogeneous nucleation is observed. Alignment between the growth direction and the thermal gradient is not perfect for every grain, suggesting crystallographic growth restriction, which implies the solidification pattern selected is columnar dendritic rather than cellular (**Figure 36E.4**).

As for the DOT investigation, diffraction trace analysis of the Al-Ag DTEM samples confirms <110> growth. Since the growth direction of the dendrites is constricted to the plane of the foil, obtaining a diffraction pattern where the zone axis is parallel with the growth direction is impossible. Instead, the sample is tilted to find an identifiable zone axis. The direction of g-vectors in the diffraction pattern and real space crystallographic vectors is parallel in cubic systems, so the diffraction spots determine the crystallographic growth direction of the dendrites (**Figure 36E.5**). Since diffraction only covers one area of the grain, dark field imaging as shown in **Figure 36E.6**, was implemented to ensure the entirety of the grain is crystallographically consistent.

36E.3.2 TEM of Al-Ge DTEM

In contrast with the Al-Ag DTEM foils, the Al-Ge DTEM foils are hypereutectic relative to the equilibrium and metastable phase diagrams. Consequentially, solidification begins with homogeneous nucleation of Ge-rich β particles (**Figure 36E.7**). As the β particles grow, Al is rejected into the liquid. Once sufficient Al is in the liquid, columnar Al-rich α dendrites grow and reject Ge into the interdendritic liquid (**Figure 36E.8**). It is currently unknown how the α dendrites form, as typical partitioning during solidification will not cause the liquid composition to cross the eutectic point. STEM-EDS was used to find the bulk composition by scanning areas in the unmelted amorphous sputtered region and averaging over the points. The composition of the α dendrites and interdendritic was also checked with STEM-EDS line scans; the growth of α dendrites in a hypereutectic alloy is not a measurement error. The growth orientation of an α dendrite was evaluated with the same diffraction trace analysis method as the columnar dendrites in the Al-Ag DTEM sample (**Figure 36E.9**), but with another pattern to capture the orientation of a secondary arm. Crystallographic growth direction was not consistent between the primary arm and secondary arm of the dendrite analyzed. While the secondary arm showed <110> growth, the primary arm was somewhere between <311> and <100>. This phenomenon might seem to suggest a discontinuity in the growing dendrite, but dark field imaging was employed similarly to the Al-Ag samples to confirm the dendrite is consistently oriented. The inconsistent growth orientation is explained by the decreased interfacial energy anisotropy associated with DOT. Typical systems not experiencing DOT will strongly select for a particular orientation due to higher anisotropy, but DOT systems have overall weaker interfacial energy anisotropy that allows for multiple dendrite orientations to grow simultaneously [36E.5, 36E.6].

36E.3.3 SYSWELD Simulations of Ni Spot Melts

The *in-situ* radiography obtained from the APS can measure solid-liquid interface velocities, but not thermal gradients. Predictions of solidification patterning require both parameters, so the thermal gradient is determined through simulations. The simulations for spot melt are made in the SYSWELD software package, which does not account for convection and assumes the same thermophysical properties between the solid and liquid. Parameters such as laser absorptivity and penetration depth are iterated until the simulated melt pool dimensions are similar to the melt pool observed with APS radiography. To facilitate analysis, the thermal gradient and velocity are determined along a vertical line through the center of the melt pool. This method is guaranteed to calculate the exact velocity along the vertical centerline, as solidification in the center of a spot melt proceeds directly vertical due to the symmetry. For similar symmetry reasons, the thermal gradient calculation should also represent the maximum thermal gradient along the centerline. A representative image of the data generated is shown in **Figure 36E.10**. The resulting gradient-velocity pathways are monotonically decreasing in gradient throughout solidification, but experience an initially high solidification velocity for the higher power conditions, as shown in **Figure 36E.11**. The result is caused by the keyhole formed at higher powers collapsing after the laser is shut off.

36E.4   Plans for Next Reporting Period

As part of the LRGF, two residency periods at NNSA national labs are required. The first of these two residency periods will be at LANL starting in the Fall 2021 semester. As a result, planned research activities are significantly impacted by the desire to utilize the unique resources available at the national labs. Overall research plans include:

- Developing interatomic potentials in the Al rich side of the Al-Ag binary system to facilitate determining the solid-liquid interfacial energy anisotropy.
- Using sputtering systems to create new Al-Ag DTEM foils in anticipation of the second residency.
- Further evaluation of Al-Ge DTEM samples, especially diffraction of more α dendrites, and further TEM of Al-Ag DTEM samples.
- EBSD of R2 and R4 samples from APS.

36E.5   References

[36E.1] T. Haxhimali, A. Karma, F. Gonzales, M. Rappaz, Orientation selection in dendritic evolution, Nature, 2006

[36E.2] K. Kranjc, M. Stubicar, X-ray diffraciton study of decomposition in aluminum-silver alloys quenched from the melt, Metallurgical Transactions, 1973

[36E.3] M. Ferranta, R.D. Doherty, Influence of interfacial proeprties on the kinetics of precipitation and precipitate coarsening in aluminium-silver alloys, Acta Metallurgica, 1979

[36E.4] M. Becker, J.A. Dantzig, M. Kolbe, S.T. Wiese, F. Kargl, Dendrite orientation transition in Al-Ge alloys, Acta Materiala, 2019

[36E.5] L. Wang, J.J. Hoyt, N. Wang, N. Provatas, C.W. Sinclair, Controlling solid-liquid interfacial energy anisotropy through the isotropic liquid, Nature, 2021

[36E.6] G. Kim, T. Takaki, Y. Shibuta, S. Sakane, K. Matsuura, M. Ohno, A parametric study of morphology selection in equiaxed dendrite solidification, Computational Materials Science, 2019

36E.6   Figures and Tables

Table 36E.1: Compositions of selected alloys.

	Ni (at%)	Al (at%)	Mo (at%)	Ag (at%)
R2	balance	6.6	1.9	N/A
R4	balance	2.8	22.2	N/A
Al-10Ag	N/A	balance	N/A	10
Al-18Ag	N/A	balance	N/A	18

Table 36E.2: Summary of laser parameters used in experiments at the APS. Pulse duration was 1 ms for all spot melts. Parameters for overlapping melts are shown with a forward slash between the parameters for each.

Alloy	Beam power [W]	Raster speed [m/s]	Notes
R2 [110], R2 [111], R4[100], R4 [110]	253.9	1.6	
	139.4	0.5	
	47.8	0.1	
	82.1/82.1	Spot melt	Edge of second pool intersects middle of first
	82.1/253.9	Spot melt	
R2 [110]	517.1	1.6	
	253.9	1	
R4 [100]	517.1	1.6	
	368.3	1.6	
	253.9	Spot melt	
Al-10Ag & Al-18Ag	282.5/282.5	0.1/0.1	Re-rasters with 100% overlap
	368.3/368.3	2/2	
	282.5	0.1	
	368.3	2	
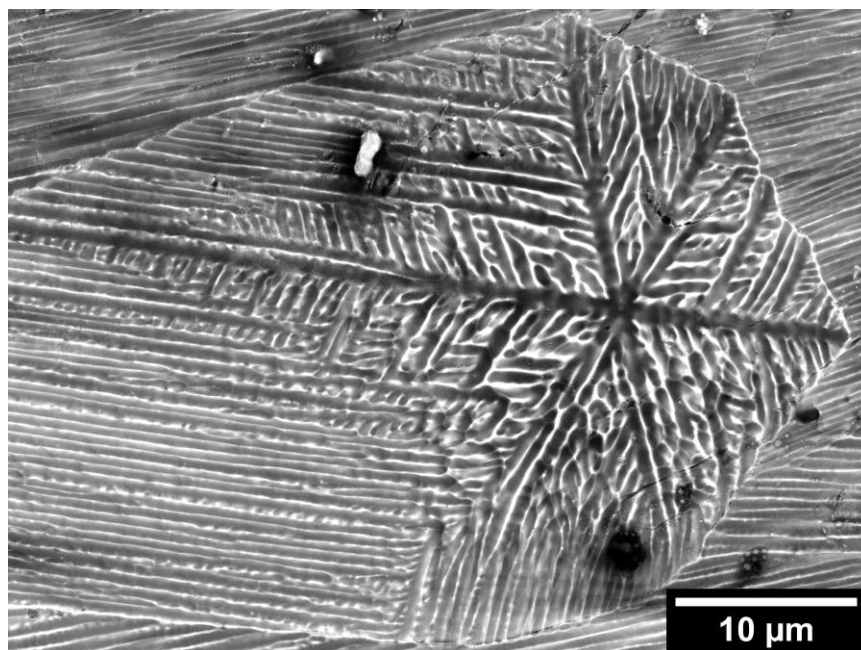
Figure 36E.1: Backscatter electron image of equiaxed dendrite in Al-Ag sample from APS, showing six primary arms contained in the same plane, indicating DOT.
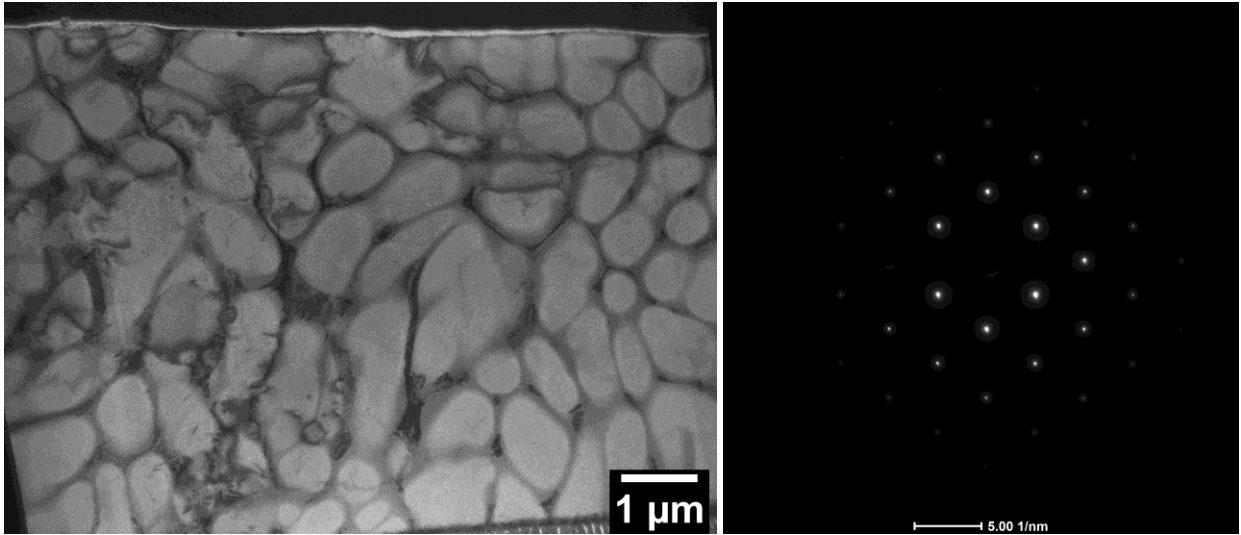
Figure36E.2: (left) Bright field TEM image of FIB lift-out of equiaxed DOT dendrite from APS Al-Ag sample formed with no tilting. The lift-out is oriented such that the projection of the growth direction on the top surface is normal to the plane of the foil. (right) Diffraction pattern down <110> zone after tilting 11.2 degrees.
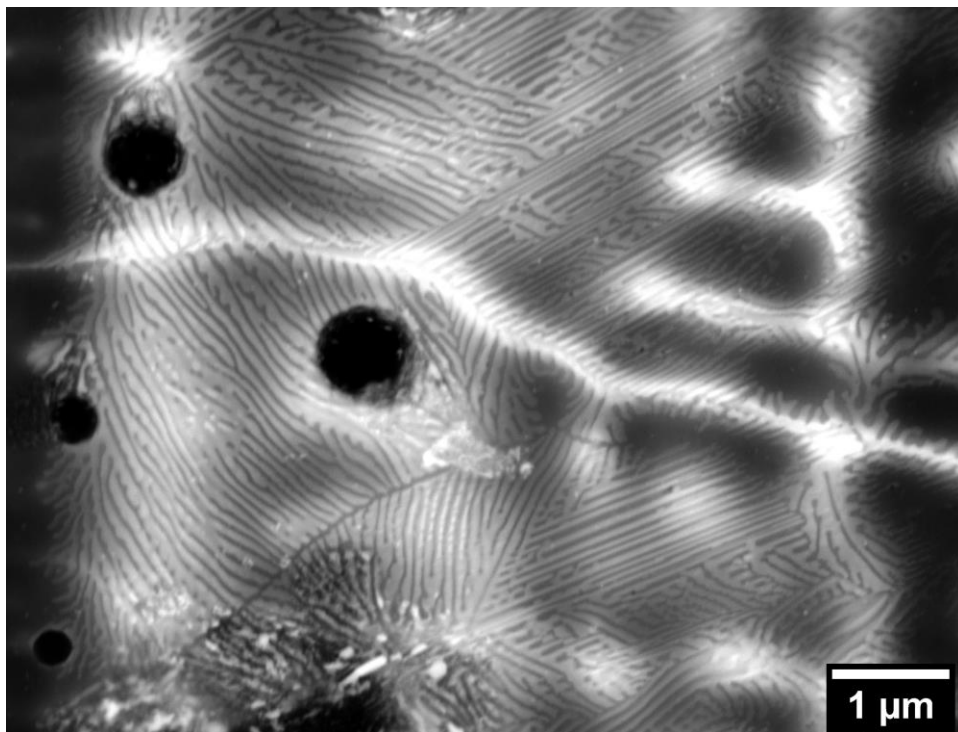

Figure 36E.3: Top-down electron backscatter image of Al-Ag sample from APS showing growth of two different γ morphologies, one platelike and the other being irregular with the development of secondary branches.
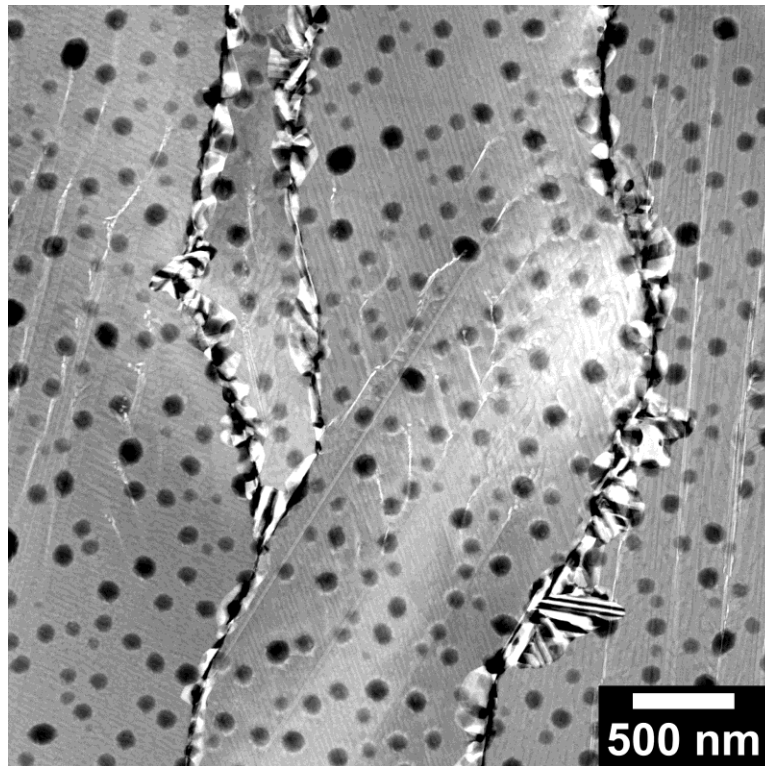
Figure 36E.4: STEM-HAADF image of a region near the edge of melt pool overlapping previous melt pool in Al-Ag, with bright lines indicating Ag rich interdendritic regions between branchless columnar dendrites. The dark spots are thinner areas of the sample believed to be associated with the possible onset of the sample dewetting from the substrate.
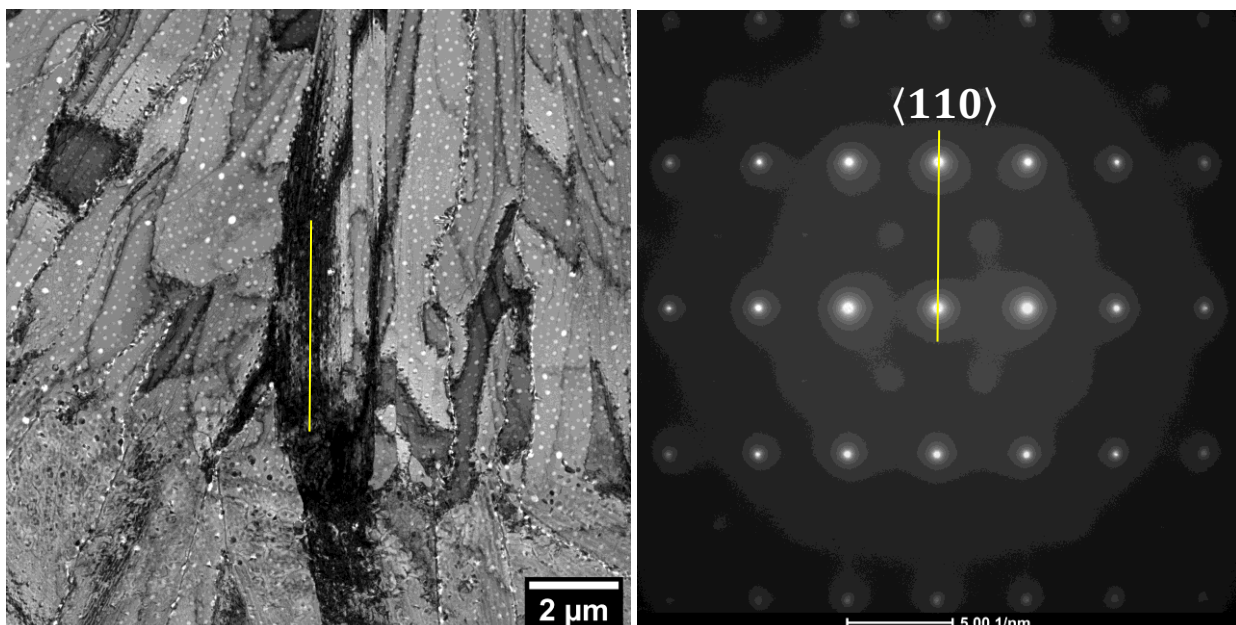

Figure 36E.5: (left) Down zone bright field of an overlapped region in Al-Ag DTEM melt pools, with the dark regions corresponding to the area analyzed in the (right) selected area diffraction pattern down the <211> zone axis.

31.6

The line inscribed on both images is the same angle and used to illustrate the growth direction of the dendrites in the darkened grain.
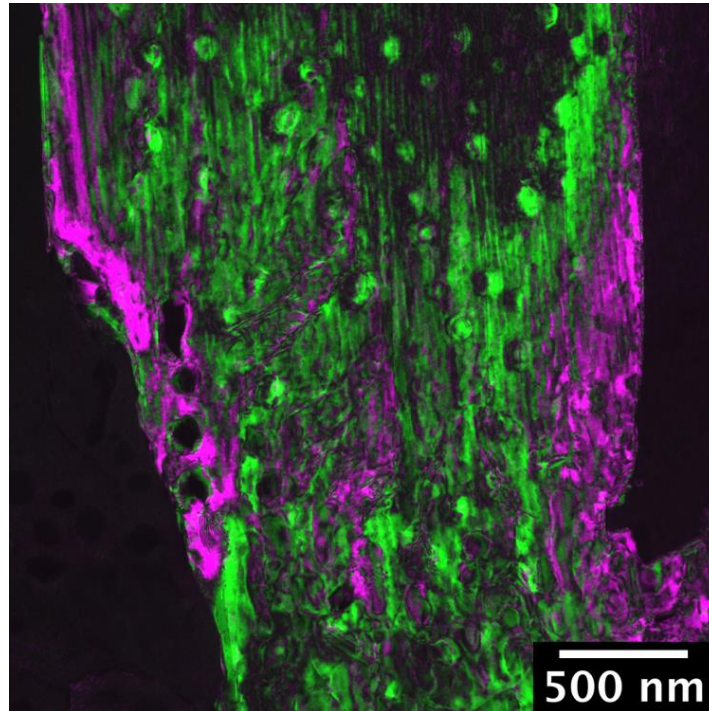
Figure 36E.6: Dark field image of the same grain shown in Figure 36E.5 (Al-Ag) with +g and –g reflections colored differently to indicate where intensity is coming from in the composite image.
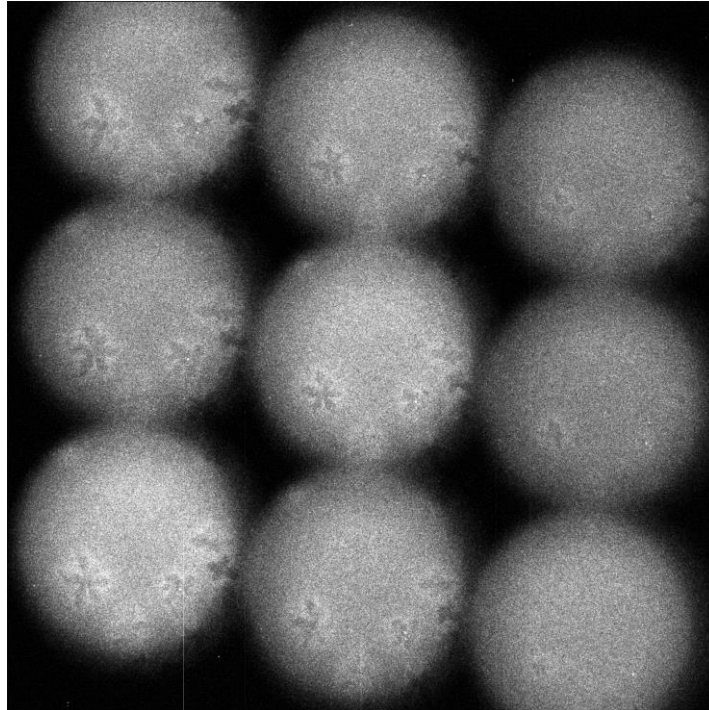

Figure 36E.7: DTEM sequence of Al-Ge foil showing homogeneous nucleation or heterogeneous nucleation on oxide contaminants of β at onset of solidification. There is a ten μs delay between images.
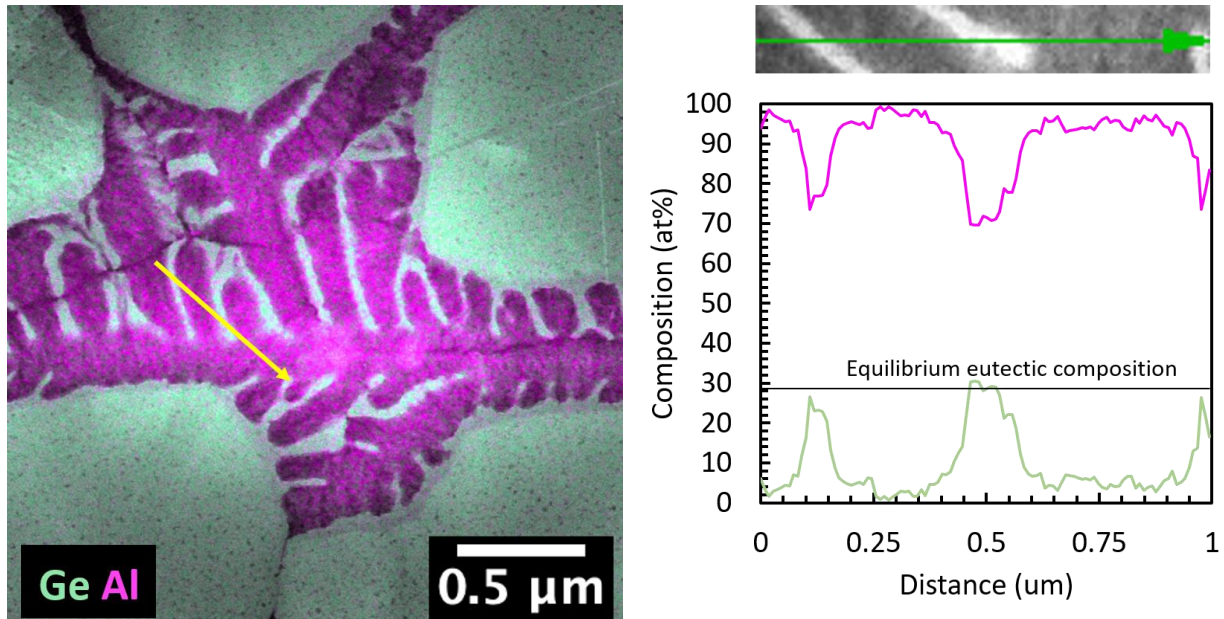
31.7

Figure 36E.8: (left) STEM-EDS map of α dendrite between primary β particles in Al-Ge. (right) STEM-EDS line scan across line indicated in other left side of figure confirming the composition of the dendrite matches that of the α Al phase.
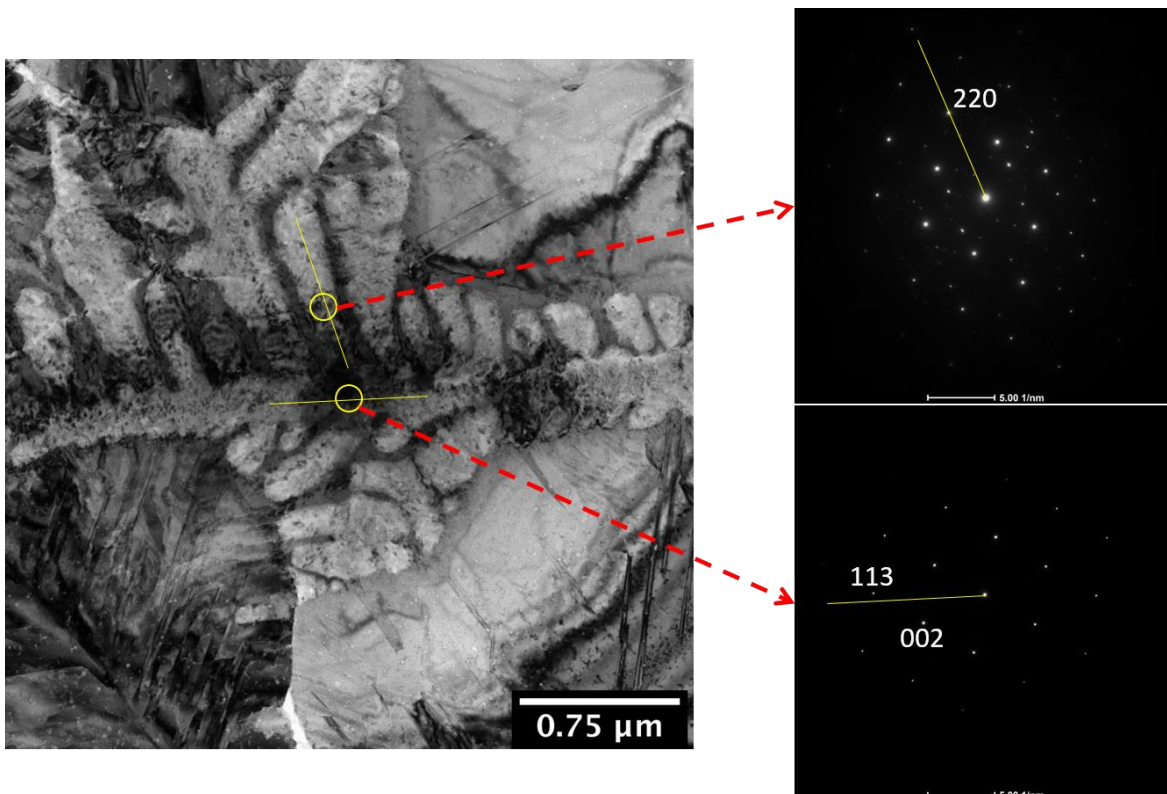

Figure 36E.9: (left) Bright field image formed without tilting of α dendrite in Al-Ge DTEM sample, (top right) SADP pattern of secondary arm showing <110> growth and (bottom right) SADP of main trunk showing growth along a crystallographic direction between the <113> and <002>.
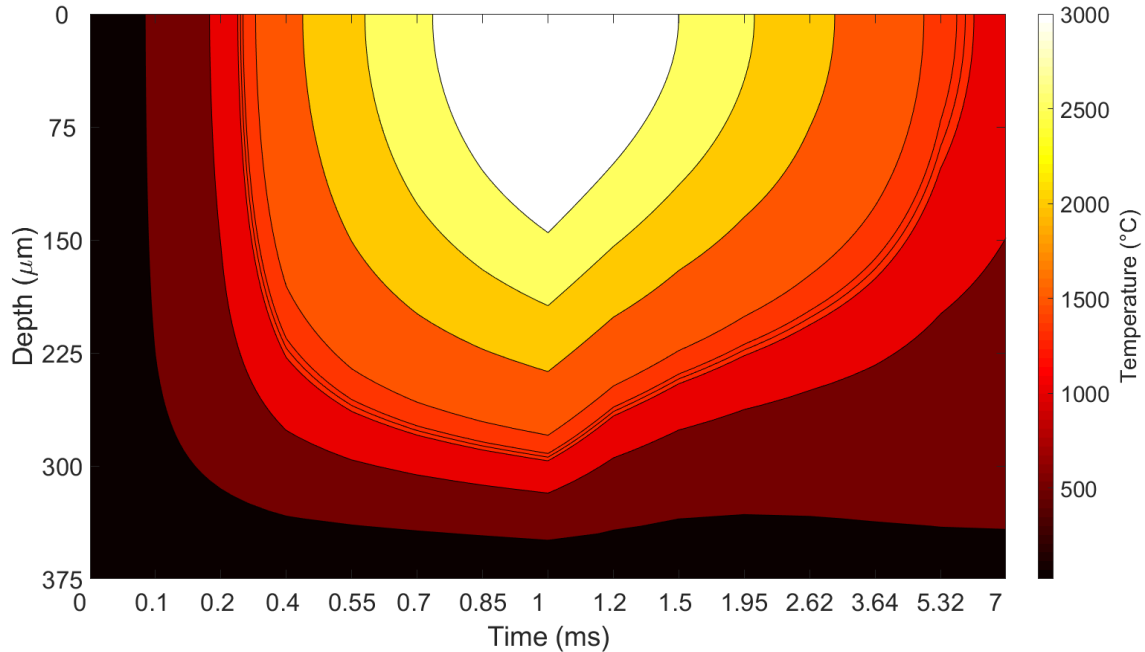
31.8

Figure 36E.10: Results from SYSWELD simulation for 197 W, 1 ms laser pulse for a Ni-base superalloy. The three closely spaced lines represent the solidus, liquidus, and mean of the two to aid in visually identifying the solid-liquid interface. This representation contains all the information needed to find gradient and velocity; partial derivatives along the vertical axis yield thermal gradient, and the instantaneous slope of the solid-liquid interface is the solidificaiton velocity.
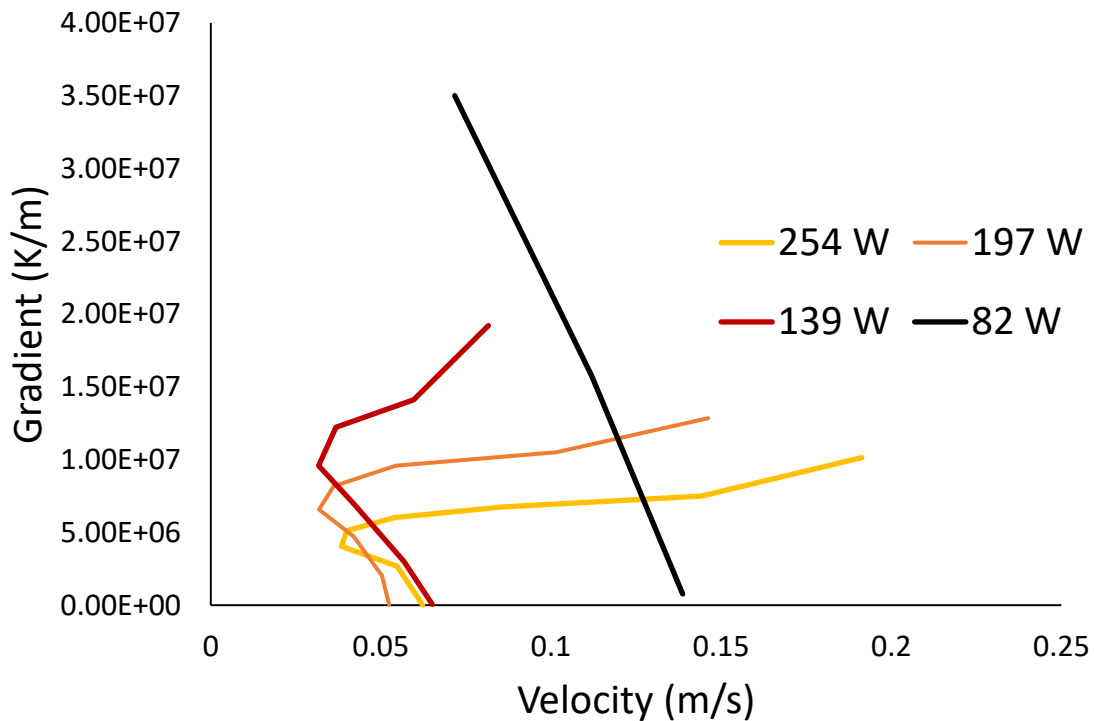

Figure 36E.11: Gradient-velocity plots for all the powers simulated using SYSWELD for a Ni-base superalloy.

31.9